Exclusive Higgs boson production with bottom quarks at hadron colliders

S. Dawson*
Physics Department, Brookhaven National Laboratory, Upton, New York 11973-5000, USA

C. B. Jackson† and L. Reina‡
Physics Department, Florida State University, Tallahassee, Florida 32306-4350, USA

D. Wackeroth§
Department of Physics, SUNY at Buffalo, Buffalo, New York 14260-1500, USA
(Received 25 November 2003; published 27 April 2004)

We present the next-to-leading order QCD corrected rate for the production of a scalar Higgs boson with a pair of high p_T bottom and antibottom quarks at the Fermilab Tevatron and at the CERN Large Hadron Collider. Results are given for both the standard model and the minimal supersymmetric standard model. The exclusive $b\bar{b}h$ production rate is small in the standard model, but it can be greatly enhanced in the minimal supersymmetric standard model for large $\tan\beta$, making $b\bar{b}h$ an important discovery mode. We find that the next-to-leading order QCD results are much less sensitive to the renormalization and factorization scales than the lowest order results, but have a significant dependence on the choice of the renormalization scheme for the bottom quark Yukawa coupling.

DOI: 10.1103/PhysRevD.69.074027 PACS number(s): 13.85.Ni, 12.38.Bx, 14.65.Fy, 14.80.Cp

I. INTRODUCTION

One of the most important problems of particle physics is to uncover the origin of the electroweak symmetry breaking. In the simplest version of the standard model (SM) of particle physics, the breaking of the electroweak symmetry introduces a single physical scalar particle, the Higgs boson, that couples to both gauge bosons and fermions. Extensions of the standard model, like the minimal supersymmetric standard model (MSSM), introduce several scalar and pseudoscalar Higgs bosons. Finding experimental evidence for one or more Higgs particles is therefore a major goal of current and future accelerators. Direct searches at the CERN e^+e^- collider LEP2 require that the SM Higgs boson mass (M_h) be heavier than 114.4 GeV (at 95% C.L.) [1], while precision electroweak measurements imply $M_h<219$ GeV (at 95% C.L.) [2]. The light scalar Higgs particle of the MSSM (h^0) should have mass between the theoretical upper bound of about 130 GeV and the experimental lower bound from LEP2, $M_{h^0}>91$ GeV (at 95% C.L., $0.5<\tan\beta<2.4$ excluded) [3]. In both cases, a Higgs boson should lie in a mass region which will certainly be explored at either the Fermilab $p\bar{p}$ Tevatron collider or at the CERN pp Large Hadron Collider (LHC).

The dominant production mechanism for a SM Higgs boson in hadronic interactions is gluon fusion. Among the subleading modes, the associated production with either electroweak gauge bosons or top quark pairs, as well as weak boson fusion, play crucial roles. The inclusion of higher order QCD corrections is in general essential to stabilize the theoretical predictions of the corresponding rates. All of them have now been calculated at next-to-leading order (NLO) [4–15] and, in the case of gluon fusion and associated production with gauge bosons, at next-to-next-to-leading order (NNLO) [16–21] in perturbative QCD.

If the standard model is not the full story, however, then other mechanisms of Higgs production become very important. Here, we focus on Higgs boson production with a pair of bottom quark and antiquark. The coupling of the Higgs boson to a $b\bar{b}$ pair is suppressed in the standard model by the small factor, m_b/v, where $v=(\sqrt{2}G_F)^{-1/2}=246$ GeV, implying that the SM Higgs production rate in association with bottom quarks is very small at both the Tevatron and the LHC. In a two Higgs doublet model or in the MSSM, however, this coupling grows with the ratio of neutral Higgs boson vacuum expectation values, $\tan\beta$, and can be significantly enhanced over the standard model coupling, leading to an observable production rate for a Higgs boson in association with bottom quarks in some regions of the parameter space.

The production of a Higgs boson in association with bottom quarks at hadron colliders has been the subject of much recent theoretical interest. At the tree level, the cross section is almost entirely dominated by $gg\to b\bar{b}h$, with only a small contribution from $q\bar{q}\to b\bar{b}h$, at both the Tevatron and the LHC. The integration over the phase space of the final state bottom quarks gives origin to large logarithms proportional to $\ln(m_b/\mu_h)$ (where $\mu_h\simeq M_h$), which arise from the splitting of an initial gluon into a pair of almost on-shell collinear bottom quarks. The use of bottom quark parton distribution functions in the proton (or antiproton) sums these large logarithms to all orders, and could therefore improve a fixed order calculation. The inclusive cross section for $b\bar{b}h$ production should then be dominated by the bottom quark fu-

*Electronic address: dawson@quark.phy.bnl.gov
†Electronic address: jackson@hep.fsu.edu
‡Electronic address: reina@hep.fsu.edu
§Electronic address: dow@ubpheno.physics.buffalo.edu

sion process $b\bar{b}\to h$, as originally proposed in Ref. [22]. Some important progress has been achieved recently. The $b\bar{b}\to h$ production process has been calculated at NNLO in QCD [23]. At NLO [24,25], the residual factorization scale dependence is quite large, but at NNLO there is almost no scale dependence. Interestingly enough the NNLO results show that the perturbative cross section is better behaved when the factorization scale is $\mu_f \simeq M_h/4$ (and the renormalization scale is $\mu_r \simeq M_h$), as expected on quite general theoretical grounds [26–29]. Moreover, the inclusive $b\bar{b}h$ cross section has been obtained at NLO in QCD via a fixed order calculation that includes the $O(\alpha_s)$ corrections to the parton level processes $gg, q\bar{q}\to b\bar{b}h$ [30–32]. The obtained results are compatible with $b\bar{b}\to h$ at NNLO, and show that there is actually no large discrepancy between the NLO fixed order calculation and the use of b-quark parton distribution functions, contrary to what was originally claimed. However, the results of the fixed order calculation have a substantial scale dependence, and a better control of the residual large uncertainty is desirable for a complete understanding of the comparison between the two approaches.

In spite of its theoretical interest, the inclusive cross section is experimentally relevant only if a Higgs boson can be detected above the background without tagging any of the outgoing bottom quarks. Higgs production from $b\bar{b}$ fusion could be useful, for instance, in a supersymmetric model with a large value of $\tan\beta$, when combined with the decays $h^0, H^0 \to \mu^+\mu^-$ and $h^0, H^0 \to \tau^+\tau^-$ [33–36]. However, even in this case, the inclusive measurement of a Higgs signal would not determine the bottom quark Yukawa coupling unambiguously, since it should be interpreted as the result of the combined action of other production channels besides $b\bar{b}\to h^0, H^0$ (e.g. $gg\to h^0, H^0$).

Requiring one or two high p_T bottom quarks in the final state reduces the signal cross section with respect to $b\bar{b}\to h$, but it also greatly reduces the background [37,36]. Moreover, it assures that the detected Higgs boson has been radiated off a bottom or antibottom quark and the corresponding cross section is therefore unambiguously proportional to the bottom quark Yukawa coupling. Using arguments similar to the ones illustrated above for the case of the inclusive cross section, one can argue that if the final state has one high p_T bottom quark then the relevant subprocess is $gb\to bh$ [24]. The cross section for $gb\to bh$ has been computed including NLO QCD corrections [38] and the residual uncertainty due to higher order QCD corrections is small. On the other hand, if the final state has two high p_T bottom quarks and a Higgs boson, then no final state bottom quark can originate from a bottom quark parton distribution function. The lowest order relevant parton level processes are unambiguously $gg\to b\bar{b}h$ and $q\bar{q}\to b\bar{b}h$. While the rate for this final state is considerably smaller than for the $b\bar{b}\to h$ and $gb\to bh$ subprocesses, the background is correspondingly reduced. The final states can be further categorized according to the decay of the Higgs boson. Existing studies have considered mostly the dominant Higgs decay channel, $h\to b\bar{b}$ [36,37,39–44], but also $h\to\tau^+\tau^-$ [37] and $h\to\mu^+\mu^-$ [45,46].

In this paper, we present the NLO QCD corrected rates and phase space distributions for the fully exclusive processes $pp, p\bar{p}\to b\bar{b}h$, where the final state includes two high p_T bottom quarks. In order to reproduce as closely as possible the currently used experimental cuts, we require the final state bottom quark/antiquark to have a transverse momentum higher than $p_T^{cut}=20$ GeV and a pseudorapidity $|\eta|\leqslant 2$ for the Tevatron and $|\eta|\leqslant 2.5$ for the LHC. The cut on $p_T^{b,b}$ greatly affects the cross section and we therefore study the dependence of the cross section on this cut. Similar results have been recently presented in Ref. [32], where however no cut on the pseudorapidity has been imposed. Our discussion will focus on assessing the uncertainty of the theoretical prediction for the exclusive $pp, p\bar{p}\to b\bar{b}h$ rates, after the full set of NLO QCD corrections has been included. We will show how the large dependence on the unphysical renormalization and factorization scales present in the lowest order (LO) calculation of the cross section is greatly reduced at NLO. Moreover, we will study the dependence on the choice of renormalization scheme for the bottom quark Yukawa coupling. While for Higgs decays and Higgs production in e^+e^- collisions using the $\overline{MS}$ definition of the bottom quark Yukawa coupling is an efficient way of improving the perturbative calculation of the corresponding rate by resumming large logarithms at all orders [47–50], this may be less compelling in the case of hadronic Higgs production. Finally, we will extend our calculation to the scalar sector of the MSSM, including the SM QCD corrections at NLO. Preliminary results of the study described in this paper have been already presented at several conferences [51].

The plan of the paper is as follows. In Sec. II we present an overview of our calculation. Since the NLO QCD corrections to $q\bar{q}, gg\to b\bar{b}h$ proceed in strict analogy to those for $q\bar{q}\to t\bar{t}h$ [10–13] and $gg\to t\bar{t}h$ [10,12,14,15], we will be very brief on details and devote more time to the discussion of the residual theoretical uncertainty, emphasizing those aspects that are characteristic of the $b\bar{b}h$ production process. For the reader's convenience we present a detailed description of the renormalization prescriptions used in a separate Appendix. Numerical results for the Tevatron and the LHC will be presented in Sec. III, for both the SM Higgs boson and the scalar MSSM Higgs bosons in some prototype regions of the model parameter space. Section IV contains our conclusions.

II. CALCULATION

A. Basics

The total cross section for $pp, p\bar{p}\to b\bar{b}h$ at $\mathcal{O}(\alpha_s^3)$ can be written as

$$\sigma_{NLO}(pp, p\bar{p}\to b\bar{b}h) = \sum_{ij}\frac{1}{1+\delta_{ij}}\int dx_1 dx_2 [\mathcal{F}_i^p(x_1,\mu)\mathcal{F}_j^{p,\bar{p}}(x_2,\mu) \times \hat{\sigma}_{NLO}^{ij}(x_1,x_2,\mu)+(1\leftrightarrow 2)], \quad (1)$$

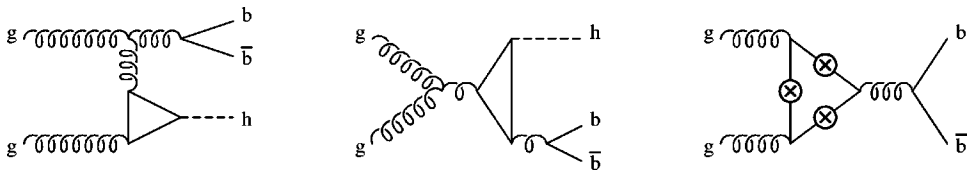

FIG. 1. Sample of diagrams corresponding to $\mathcal{O}(\alpha_s)$ virtual corrections where the Higgs boson couples to an internal fermion loop and not to the external $b\bar{b}$ pair. The circled cross denotes all possible insertion of the final state Higgs boson leg, each insertion corresponding to a different diagram.

where $\mathcal{F}_i^{p,\bar{p}}$ are the NLO parton distribution functions (PDFs) for parton i in a proton or antiproton, defined at a generic factorization scale $\mu_f=\mu$, and $\hat{\sigma}_{NLO}^{ij}$ is the $\mathcal{O}(\alpha_s^3)$ parton-level total cross section for incoming partons i and j, made of the channels $q\bar{q},gg\to b\bar{b}h$ and $(q,\bar{q})g\to b\bar{b}h(q,\bar{q})$, and renormalized at an arbitrary scale μ_r which we also take to be $\mu_r=\mu$. Throughout this paper we will always assume the factorization and renormalization scales to be equal, $\mu_r=\mu_f=\mu$. The partonic center-of-mass energy squared, s, is given in terms of the hadronic center-of-mass energy squared, s_H, by $s=x_1x_2s_H$. At both the Tevatron and the LHC, the dominant contribution is from the gluon-gluon initial state, although we include all initial states.

The NLO parton-level total cross section reads

$$\hat{\sigma}_{NLO}^{ij}(x_1,x_2,\mu)=\hat{\sigma}_{LO}^{ij}(x_1,x_2,\mu)+\delta\hat{\sigma}_{NLO}^{ij}(x_1,x_2,\mu), \tag{2}$$

where $\hat{\sigma}_{LO}^{ij}(x_1,x_2,\mu)$ is the $\mathcal{O}(\alpha_s^2)$ Born cross section, and $\delta\hat{\sigma}_{NLO}^{ij}(x_1,x_2,\mu)$ consists of the $\mathcal{O}(\alpha_s)$ corrections to the Born cross sections for $gg,q\bar{q}\to b\bar{b}h$ and of the tree level $(q,\bar{q})g\to b\bar{b}h(q,\bar{q})$ processes, including the effects of mass factorization.

The evaluation of $\hat{\sigma}_{NLO}^{ij}$ proceeds along the same lines as the corresponding calculation for $t\bar{t}h$ production [10–15] and we refer to Refs. [13,15] for a detailed description of the techniques used in our calculation. We notice that, in view of the generalization to the MSSM with a very enhanced bottom quark Yukawa coupling, both top and bottom quark loops need to be considered in those virtual diagrams where the Higgs boson couples directly to a closed loop of fermions, a sample of which is illustrated in Fig. 1.

Contrary to the case of $t\bar{t}h$ production, the NLO cross section for $b\bar{b}h$ production depends significantly on the renormalization scheme used for the bottom quark Yukawa coupling, i.e. for the bottom quark mass appearing in $g_{b\bar{b}h}=m_b/v$. In our calculation of the NLO $p\bar{p},pp\to b\bar{b}h$ cross section we have considered, for the renormalization of the bottom quark Yukawa coupling, both the on-shell and the $\overline{MS}$ subtraction schemes (in the $t\bar{t}h$ case we only used the on-shell top quark renormalized mass everywhere [15]). The $\overline{MS}$ scheme results in a running bottom quark Yukawa coupling and potentially gives better control over higher order contributions beyond the 1-loop corrections. We will study the origin and magnitude of the residual scheme dependence in Secs. II B and III A.

B. Renormalization scheme dependence

The ultraviolet (UV) divergences arising from self-energy and vertex $\mathcal{O}(\alpha_s)$ virtual corrections to $q\bar{q},gg\to b\bar{b}h$ are regularized in $d=4-2\epsilon$ dimensions and renormalized by introducing counterterms for the wave functions of the external fields [$\delta Z_2^{(q)}$ (for $q=u,d,c,s$), $\delta Z_2^{(b)}$ for the bottom quark, and δZ_3 for the gluon], for the bottom quark mass, δm_b, and for the bottom quark Yukawa and strong coupling constants, $\delta g_{b\bar{b}h}$ and δZ_{α_s}. We follow the same renormalization prescription and notation adopted in Refs. [13,15] for the NLO $t\bar{t}h$ inclusive cross section. Consequently, we fix the wave-function renormalization constants of the external massless quark fields, $\delta Z_2^{(q)}$, using on-shell subtraction, while we define the wave function renormalization constant of external gluons, δZ_3, using the $\overline{MS}$ subtraction scheme and the α_s renormalization constant, δZ_{α_s}, using the $\overline{MS}$ scheme modified to decouple the top quark [52,53]. Explicit expressions for $\delta Z_2^{(q)}$, δZ_3, and δZ_{α_s} can be found in Refs. [13,15] and in the Appendix.

However, given the large sensitivity of the $\overline{MS}$ bottom quark mass to the renormalization scale and given the prominent role it plays in the $b\bar{b}h$ production cross section through the overall bottom quark Yukawa coupling, we investigate here the dependence of the final results on the renormalization prescription adopted for the bottom quark. We consider both the on-shell (*OS*) and $\overline{MS}$ subtraction schemes, for both the bottom quark mass and wave function renormalization constants.

When using the *OS* subtraction scheme, we fix the wave function renormalization constant of the external bottom quark field, $(\delta Z_2^{(b)})_{OS}$, and the mass renormalization constant, $(\delta m_b)_{OS}$, by requiring that

$$\hat{\Sigma}_b(\not{p}=m_b)=0; \qquad \lim_{\not{p}\to m_b}\frac{\hat{\Sigma}_b(\not{p})}{\not{p}-m_b}=0, \tag{3}$$

where

$$\hat{\Sigma}_b=(\not{p}-m_b)(\Sigma_V+\delta Z_2^{(b)})+m_b\left(\Sigma_S+\Sigma_V-\frac{\delta m_b}{m_b}\right) \tag{4}$$

denotes the renormalized bottom quark self-energy at 1-loop in QCD, expressed in terms of the vector, Σ_V, and scalar, Σ_S, parts of the unrenormalized self-energy, and of the mass and wave function renormalization constants. Using Eq. (3) in $d=4-2\epsilon$ dimensions one finds

$$(\delta Z_2^{(b)})_{OS} = -\frac{\alpha_s}{4\pi} C_F \left(\frac{4\pi\mu^2}{m_b^2}\right)^{\epsilon} \Gamma(1+\epsilon)\left(\frac{1}{\epsilon_{UV}} + 4 + \frac{2}{\epsilon_{IR}}\right), \tag{5}$$

$$\left(\frac{\delta m_b}{m_b}\right)_{OS} = -\frac{\alpha_s}{4\pi} C_F \left(\frac{4\pi\mu^2}{m_b^2}\right)^{\epsilon} \Gamma(1+\epsilon)\left(\frac{3}{\epsilon_{UV}} + 4\right), \tag{6}$$

where $C_F=(N^2-1)/2/N$ and $N=3$ is the number of colors. We have explicitly distinguished between ultraviolet and infrared divergences. The infrared divergences are cancelled between virtual and real soft and collinear contributions according to the pattern outlined in Refs. [13,15], to which we refer for more details.

In the $\overline{MS}$ scheme, the bottom quark renormalization constants are fixed by requiring that they cancel the UV divergent parts of the bottom quark self-energy $\hat{\Sigma}_b$ of Eq. (4), i.e.

$$(\delta Z_2^{(b)})_{\overline{MS}} = -\frac{\alpha_s}{4\pi} C_F (4\pi)^{\epsilon} \Gamma(1+\epsilon) \frac{1}{\epsilon_{UV}}, \tag{7}$$

$$\left(\frac{\delta m_b}{m_b}\right)_{\overline{MS}} = -\frac{\alpha_s}{4\pi} C_F (4\pi)^{\epsilon} \Gamma(1+\epsilon) \frac{3}{\epsilon_{UV}}. \tag{8}$$

According to the LSZ prescription [54], one also needs to consider the insertion of the renormalized one-loop self-energy corrections on the external bottom quark legs. While these terms are zero in the *OS* scheme [see Eq. (3)], they are not zero in the $\overline{MS}$ scheme. Together with $(\delta Z_2^{(b)})_{\overline{MS}}$, their contribution to the NLO cross section equals the contribution of the wave function counterterm in the *OS* scheme, $(\delta Z_2^{(b)})_{OS}$, as expected from the LSZ prescription itself. The cross section does not depend on the renormalization of the external particle wave functions.

We therefore focus on the scheme dependence induced by the choice of different subtraction schemes for the bottom quark mass. We note that the bottom quark mass counterterm has to be used twice: once to renormalize the bottom quark mass appearing in internal propagators and once to renormalize the bottom quark Yukawa coupling. Indeed, if one considers only QCD corrections, the counterterm for the bottom quark Yukawa coupling,

$$\delta g_{b\bar{b}h} = \frac{\delta m_b}{v}, \tag{9}$$

coincides with the counterterm for the bottom quark mass, since the SM Higgs vacuum expectation value v is not renormalized at 1-loop in QCD. This stays true when we generalize the $g_{b\bar{b}h}$ coupling from the SM to the case of the scalar Higgs bosons of the MSSM.

At 1-loop order in QCD, the relation between the pole mass, m_b, and the $\overline{MS}$ mass, $\overline{m}_b(\mu)$, is indeed determined by the difference between the *OS* and $\overline{MS}$ bottom mass counterterms, $(\alpha_s/4\pi)\delta CT$, since

$$\overline{m}_b(\mu) = m_b\left\{1 - \frac{\alpha_s(\mu)}{4\pi} C_F\left[3\ln\left(\frac{\mu^2}{m_b^2}\right) + 4\right]\right\} \equiv m_b\left[1 - \frac{\alpha_s(\mu)}{4\pi}\delta CT(\mu)\right]. \tag{10}$$

Adopting the *OS* or $\overline{MS}$ prescription consists of using either Eq. (6) or Eq. (8) for the bottom mass counterterms while substituting m_b or $\overline{m}_b(\mu)$ respectively in both the bottom quark propagator and Yukawa coupling. At $\mathcal{O}(\alpha_s^3)$ the two prescriptions give identical results. Indeed, replacing m_b by $\overline{m}_b(\mu)$ in the Yukawa coupling adds a term

$$-\frac{\alpha_s(\mu)}{2\pi}\delta CT(\mu)\hat{\sigma}_{LO} + \mathcal{O}(\alpha_s^4) \tag{11}$$

to the NLO parton level cross section, which compensates exactly for the difference in the OS and $\overline{MS}$ counterterms. On the other hand, using the $\overline{MS}$ mass in the bottom quark propagator,

$$\frac{i}{\not{p} - \overline{m}_b(\mu)} = \frac{i}{\not{p} - m_b}\left[1 + i m_b \frac{\alpha_s}{4\pi}\delta CT(\mu)\frac{i}{\not{p} - m_b}\right] + \mathcal{O}(\alpha_s^2), \tag{12}$$

of the LO cross section leads to an extra contribution to the $\overline{MS}$ NLO cross section which, together with the $\overline{MS}$ mass counterterm insertions into the internal bottom quark propagators (see diagrams S_1 in Fig. 2 of Ref. [13] and S_2, S_3, and S_4 in Fig. 2 of Ref. [15]), coincides with the corresponding mass counterterm insertions in the *OS* scheme at $\mathcal{O}(\alpha_s^3)$.

Therefore, using OS or $\overline{MS}$ to define the renormalized bottom quark mass at $\mathcal{O}(\alpha_s^3)$ is perturbatively consistent, the difference between the two schemes being of higher order and hence, strictly speaking, part of the theoretical uncertainty of the NLO calculation. One notices however that some of the large logarithms involved in the renormalization procedure of the NLO cross section come from the renormalization of the bottom quark mass, and are nicely factored out by using the $\overline{MS}$ bottom mass in the bottom quark Yukawa coupling [see Eq. (10)]. Therefore one should consider reorganizing the perturbative expansion in terms of leading logarithms [of the form $\alpha_s^n(\mu)\ln^n(\mu^2/m_b^2)$] or next-to-leading-logarithms [of the form $\alpha_s^n(\mu)\ln^{n-1}(\mu^2/m_b^2)$, for $\mu \simeq M_h$], as obtained by replacing the $\overline{MS}$ bottom mass in the Yukawa coupling by the corresponding 1-loop or 2-loop renormalization group improved $\overline{MS}$ masses,

$$\overline{m}_b(\mu)_{1l} = m_b\left[\frac{\alpha_s(\mu)}{\alpha_s(m_b)}\right]^{c_0/b_0}, \tag{13}$$

$$\overline{m}_b(\mu)_{2l}=m_b\left[\frac{\alpha_s(\mu)}{\alpha_s(m_b)}\right]^{c_0/b_0}\left[1+\frac{c_0}{b_0}(c_1-b_1)[\alpha_s(\mu)-\alpha_s(m_b)]\right]\left(1-\frac{4}{3}\frac{\alpha_s(m_b)}{\pi}\right), \quad (14)$$

where

$$b_0=\frac{1}{4\pi}\left(\frac{11}{3}N-\frac{2}{3}n_{lf}\right), \quad c_0=\frac{1}{\pi}, \quad (15)$$

$$b_1=\frac{1}{2\pi}\frac{51N-19n_{lf}}{11N-2n_{lf}}, \quad c_1=\frac{1}{72\pi}(101N-10n_{lf}), \quad (16)$$

are the one and two loop coefficients of the QCD β-function and mass anomalous dimension γ_m, while $N=3$ is the number of colors and $n_{lf}=5$ is the number of light flavors.

In both Higgs boson decays to heavy quarks and Higgs boson production with heavy quarks in e^+e^- collisions, using Eq. (13) at LO and Eq. (14) at NLO in the Yukawa coupling proves to be a very powerful way to stabilize the perturbative calculation of the cross section [47]. The difference between LO and NLO rates is reduced and the dependence on the renormalization and factorization scales at NLO is very mild, indicating a very small residual theoretical error or equivalently a very good convergence of the perturbative expansion of the corresponding rate. This is due to the fact that in these cases to a large extent the $\mathcal{O}(\alpha_s)$ QCD corrections amount to a renormalization of the heavy quark mass in the Yukawa coupling. In more complicated cases, like the case of the hadronic cross section discussed in this paper, the previous argument is not automatically true.

Using the *OS* or $\overline{MS}$ bottom quark mass mainly affects the Yukawa coupling. Therefore, in the hadronic case, we will look at the different behavior of the NLO cross section when the bottom quark Yukawa coupling is renormalized either in the *OS* or in the $\overline{MS}$ scheme, keeping the bottom quark pole mass everywhere else. Figure 2 of Sec. III shows the renormalization and factorization scale dependence of the LO and NLO cross sections for $pp,p\bar{p}\to b\bar{b}h$ obtained using in the Yukawa coupling either the pole mass m_b or the $\overline{MS}$ running mass $\overline{m}_b(\mu)$ in Eq. (13) (at LO) and Eq. (14) (at NLO). The use of $\overline{m}_b(\mu)$ both at LO and NLO seems to improve the perturbative calculation of the cross section, since the NLO $\overline{MS}$ cross section is better behaved than the NLO *OS* cross section at low scales and since the difference between the LO and NLO cross section is smaller when the bottom quark Yukawa coupling is renormalized in the $\overline{MS}$ scheme than in the *OS* scheme. However, both the OS and the $\overline{MS}$ cross sections have very well defined regions of minimum sensitivity to the variation of the renormalization/factorization scale and these regions do not quite overlap. The difference between the *OS* and $\overline{MS}$ results at the plateau should rather be interpreted, in the absence of a NNLO calculation, as an upper bound on the theoretical uncertainty.

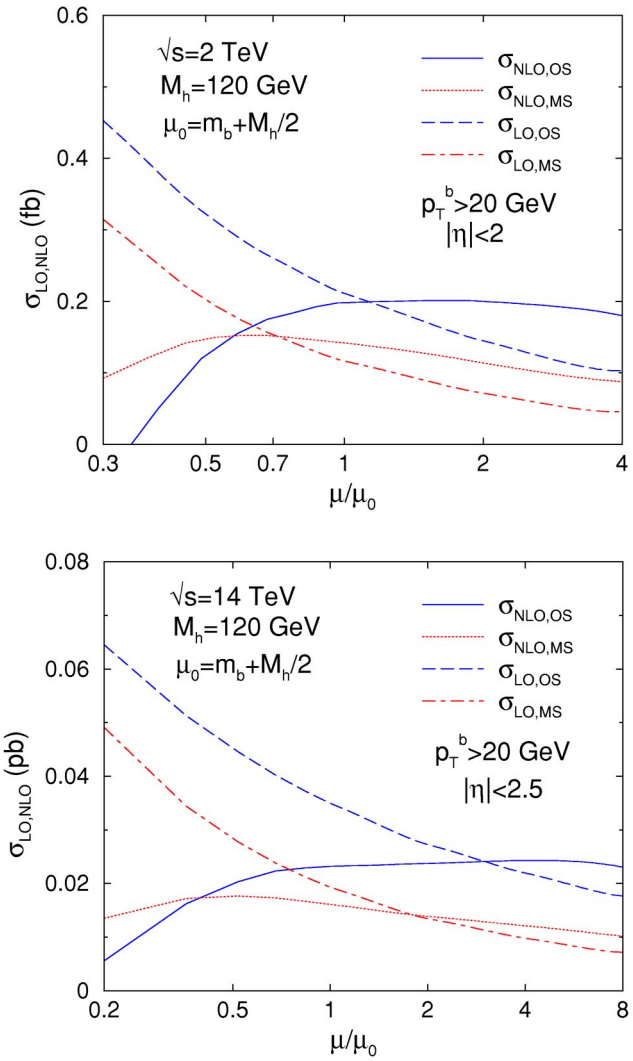

FIG. 2. σ_{NLO} and σ_{LO} for $p\bar{p}\to b\bar{b}h$ at $\sqrt{s}=2$ TeV (top) and for $pp\to b\bar{b}h$ at $\sqrt{s}=14$ TeV (bottom) as a function of the renormalization/factorization scale μ, for $M_h=120$ GeV. The curves labeled $\sigma_{LO,OS}$ and $\sigma_{NLO,OS}$ use the *OS* renormalization scheme for the bottom quark Yukawa coupling, while the curves labeled $\sigma_{LO,MS}$ and $\sigma_{NLO,MS}$ use the $\overline{MS}$ scheme.

The origin of the large difference between the *OS* and $\overline{MS}$ NLO cross sections illustrated in Fig. 2 can be understood by studying the numerical effect of the higher order terms that are included in the NLO $\overline{MS}$ cross section when $\overline{m}_b(\mu)$ is used in the Yukawa coupling. The parton level NLO cross sections for $ij\to b\bar{b}h$ $(ij=q\bar{q},gg)$ in the *OS* and $\overline{MS}$ prescription explained above can be written as

$$\hat{\sigma}^{ij}_{NLO,OS}(x_1,x_2,\mu)=m_b^2\alpha_s^2(\mu)\left\{g^{ij}_{LO}(x_1,x_2)+\frac{\alpha_s(\mu)}{4\pi}\left[g^{ij}_{NLO}(x_1,x_2,\mu)-2g^{ij}_{LO}(x_1,x_2)\delta CT(\mu)+\frac{m_t}{m_b}g^{ij}_{cl}(x_1,x_2)\right]\right\}, \quad (17)$$

$$\hat{\sigma}^{ij}_{NLO,\overline{MS}}(x_1,x_2,\mu) = \overline{m}_b^2(\mu)\alpha_s^2(\mu)\left\{ g^{ij}_{LO}(x_1,x_2) + \frac{\alpha_s(\mu)}{4\pi}\left[g^{ij}_{NLO}(x_1,x_2,\mu) + \frac{m_t}{\overline{m}_b(\mu)} g^{ij}_{cl}(x_1,x_2)\right]\right\}, \quad (18)$$

where the dependence on the renormalization scale is explicitly given. $\alpha_s(\mu)$ is the 2-loop strong coupling, m_b is the bottom quark pole mass, and $\overline{m}_b(\mu)$ is the bottom quark $\overline{MS}$ mass. g^{ij}_{LO}, g^{ij}_{NLO} and g^{ij}_{cl} have been defined in such a way that they are the same in the *OS* and the $\overline{MS}$ schemes. They correspond respectively to the $\mathcal{O}(\alpha_s^2)(g^{ij}_{LO})$ and $\mathcal{O}(\alpha_s^3)$ (g^{ij}_{NLO}) contributions to the NLO QCD cross section, from which we have singled out the $\mathcal{O}(\alpha_s)$ virtual corrections where the Higgs boson couples to a top quark in a closed fermion loop (g^{ij}_{cl}, see, e.g., diagrams in Fig. 1) as well as $\delta CT(\mu)$, i.e. the difference between the *OS* and $\overline{MS}$ bottom mass counterterms defined in Eq. (10). Using Eqs. (17) and (18), one can easily verify that the difference between the parton level NLO cross sections obtained by using either the *OS* or the $\overline{MS}$ scheme for the bottom quark Yukawa coupling is, as expected, of higher order in α_s, i.e.

$$\hat{\Delta} = \hat{\sigma}^{ij}_{NLO,OS} - \hat{\sigma}^{ij}_{NLO,\overline{MS}} = \alpha_s^2(\mu) g^{ij}_{LO}(x_1,x_2)\left[m_b^2 - \overline{m}_b^2(\mu) - m_b^2 \frac{\alpha_s(\mu)}{2\pi}\delta CT(\mu)\right] + \frac{\alpha_s^3(\mu)}{4\pi}[m_b^2 - \overline{m}_b^2(\mu)]\left[g^{ij}_{NLO}(x_1,x_2,\mu) + \frac{m_t}{m_b + \overline{m}_b(\mu)} g^{ij}_{cl}(x_1,x_2)\right]. \quad (19)$$

The term in the first bracket of Eq. (19) vanishes at $\mathcal{O}(\alpha_s^3)$, as can be easily verified by using Eq. (10). Hence all the terms in Eq. (19) only contribute at $O(\alpha_s^4)$ and higher. However, while the first term is in general quite small, the term proportional to $g^{ij}_{NLO}(x_1,x_2,\mu)$ can be large and has a nontrivial scale dependence that we can formally write as

$$g^{ij}_{NLO}(x_1,x_2,\mu) = g^{ij}_1(x_1,x_2) + \tilde{g}^{ij}_1(x_1,x_2)\ln\left(\frac{\mu^2}{s}\right). \quad (20)$$

From renormalization group arguments [13,15] one can see that $\tilde{g}^{ij}_1(x_1,x_2)$ is given by

$$\tilde{g}^{ij}_1(x_1,x_2) = 2\left\{ (4\pi b_0 + 4) g^{ij}_{LO}(x_1,x_2) - \sum_k \left[\int_\rho^1 dz_1 P_{ik}(z_1) g^{kj}_{LO}(x_1 z_1, x_2) + \int_\rho^1 dz_2 P_{jk}(z_2) g^{ik}_{LO}(x_1, x_2 z_2)\right]\right\}, \quad (21)$$

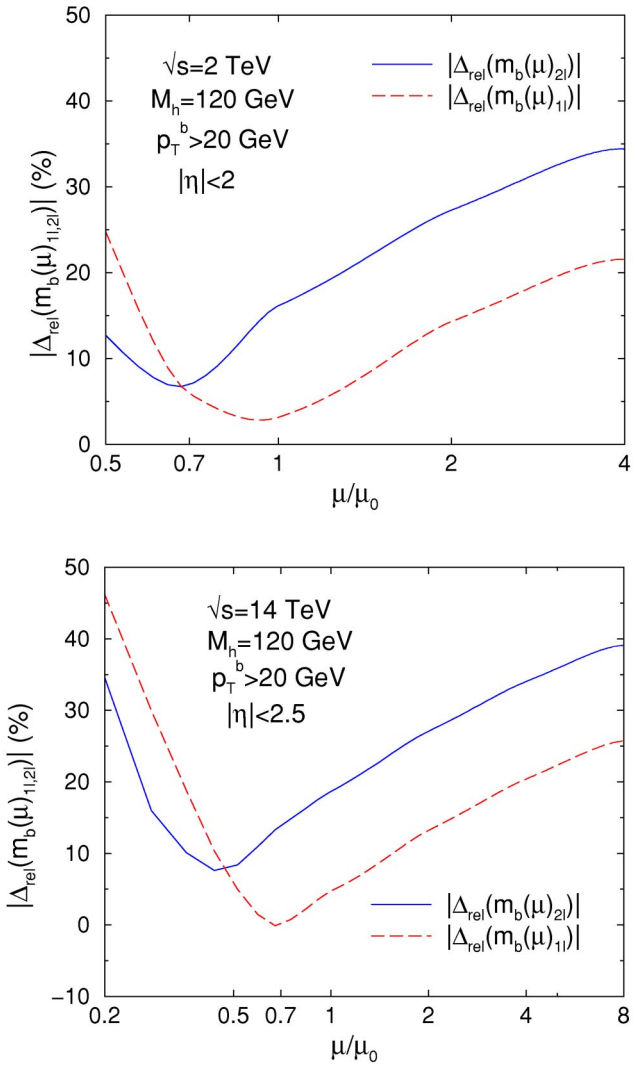

FIG. 3. The absolute value of the relative difference $\Delta_{rel} = (\sigma_{NLO,OS} - \sigma_{NLO,\overline{MS}})/(\sigma_{NLO,OS} + \sigma_{NLO,\overline{MS}})$ for $p\overline{p} \to b\overline{b}h$ at $\sqrt{s} = 2$ TeV (top) and for $pp \to b\overline{b}h$ at $\sqrt{s} = 14$ TeV (bottom) as a function of the renormalization/factorization scale μ, for $M_h = 120$ GeV. The *OS* and $\overline{MS}$ labels refer to the renormalization scheme chosen for the bottom quark Yukawa coupling. The curves labeled as $\Delta_{rel}(\overline{m}_b(\mu)_{1l})$ and $\Delta_{rel}(\overline{m}_b(\mu)_{2l})$ use the $\overline{MS}$ bottom quark Yukawa coupling with the 1-loop running mass of Eq. (13) and the 2-loop running mass of Eq. (14), respectively, in the calculation of $\sigma_{NLO,\overline{MS}}$.

where $\rho = (2m_b + M_h)^2/s$, $P_{ij}(z)$ denotes the lowest-order regulated Altarelli-Parisi splitting function [55] of parton i into parton j, when j carries a fraction z of the momentum of parton i (see e.g. Sec. V of Ref. [15]), and b_0 is given in Eq. (15). As a result, $\hat{\Delta}$, defined in Eq. (19), turns out to have a nontrivial scale dependence and, thus, the difference between the NLO hadronic cross section calculated with the *OS* or with the $\overline{MS}$ definition of the bottom quark Yukawa coupling can be numerically quite significant for some values of the renormalization/factorization scale, as we will illustrate in Sec. III (see Figs. 2 and 3).

III. NUMERICAL RESULTS

Our numerical results are obtained using CTEQ5M parton distribution functions for the calculation of the NLO cross section, and CTEQ5L parton distribution functions for the calculation of the lowest order cross section [56]. The NLO (LO) cross section is evaluated using the 2-loop (1-loop) evolution of $\alpha_s(\mu)$ with $\alpha_s^{NLO}(M_Z)=0.118$. The bottom quark pole mass is taken to be $m_b=4.6$ GeV. In the OS scheme the bottom quark Yukawa coupling is calculated as $g_{b\bar{b}h}=m_b/v$, while in the $\overline{MS}$ scheme as $g_{b\bar{b}h}(\mu)=\overline{m_b}(\mu)/v$, where we use $\overline{m_b}(\mu)_{1l}$ from Eq. (13) for σ_{LO} and $\overline{m_b}(\mu)_{2l}$ from Eq. (14) for σ_{NLO}.

We evaluate the fully exclusive LO and NLO cross sections for $b\bar{b}h$ production by requiring that the transverse momentum of both final state bottom and antibottom quarks be larger than 20 GeV ($p_T^b>20$ GeV), and that their pseudorapidity satisfy the condition $|\eta_b|<2$ for the Tevatron and $|\eta_b|<2.5$ for the LHC. This corresponds to an experiment measuring the Higgs decay products along with two high p_T bottom quark jets that are clearly separated from the beam. Furthermore, we present LO and NLO transverse momentum and pseudorapidity distributions. In order to better simulate the detector response, the gluon and the bottom/antibottom quarks are treated as distinct particles only if the separation in the azimuthal angle-pseudorapidity plane is $\Delta R>0.4$. For smaller values of ΔR, the four momentum vectors of the two particles are combined into an effective bottom/antibottom quark momentum four-vector.

A. Standard model results

In Fig. 2 we show, for $M_h=120$ GeV, the dependence of the LO and NLO cross sections for $p\bar{p}\to b\bar{b}h$ at the Tevatron (top) and for $pp\to b\bar{b}h$ at the LHC (bottom) on the unphysical factorization and renormalization scale, μ, when using either the *OS* or the $\overline{MS}$ renormalization schemes for the bottom quark Yukawa coupling. In both the *OS* and $\overline{MS}$ schemes the stability of the cross section is greatly improved at NLO, given the much milder scale dependence with respect to the corresponding LO cross section. The results presented in Fig. 2 are obtained by setting $\mu=\mu_r=\mu_f$, i.e. by identifying the renormalization (μ_r) and factorization (μ_f) scales. We have checked that varying them independently does not affect the results significantly. By varying the scale μ in the ranges $0.7\mu_0<\mu<4\mu_0$ (Tevatron) and $0.5\mu_0<\mu<8\mu_0$ (LHC), when using the *OS* scheme for the bottom quark Yukawa coupling, and in the ranges $0.4\mu_0<\mu<2\mu_0$ (Tevatron) and $0.2\mu_0<\mu<2\mu_0$ (LHC) when using the $\overline{MS}$ scheme, i.e. in the plateau regions, the value of the NLO cross section varies by at most 15–20 % (where $\mu_0=m_b+M_h/2$).

As can be seen in Fig. 2, the cross section calculated with $g_{b\bar{b}h}$ in the $\overline{MS}$ scheme shows a better perturbative behavior, since the difference between σ_{LO} and σ_{NLO} is smaller. This is in part due to the fact that the LO cross section is calculated using $\overline{m_b}(\mu)_{1l}$ and therefore already contains some of the corrections from the renormalization of the bottom quark Yukawa coupling that appear in the NLO cross section as well as at higher order. This observation seems to justify the use of $\overline{m_b}(\mu)_{1l}$ at LO and $\overline{m_b}(\mu)_{2l}$ at NLO. One also observes that the $\overline{MS}$ NLO cross section is better behaved at low values of the renormalization/factorization scales. At the same time, both the *OS* and $\overline{MS}$ cross sections show well defined but distinct regions of least sensitivity to the renormalization/factorization scale. In both cases this happens in the region where the LO and NLO cross section are closer. The variation of the NLO cross section with μ about its point of least sensitivity to the renormalization/factorization scale is almost the same whether one uses the *OS* or $\overline{MS}$ schemes for the bottom quark Yukawa coupling. This indicates that the running of the Yukawa coupling is not the only important factor to determine the overall perturbative stability of the NLO cross section.

As discussed in Sec. II B, the numerical difference between the two renormalization schemes can be significant. This is illustrated in Fig. 3 where we plot the absolute value of the normalized relative difference Δ_{rel} between the hadronic cross sections $\sigma_{NLO,OS}$ and $\sigma_{NLO,\overline{MS}}$, $\Delta_{rel}=(\sigma_{NLO,OS}-\sigma_{NLO,\overline{MS}})/(\sigma_{NLO,OS}+\sigma_{NLO,\overline{MS}})$, at both the Tevatron and the LHC. The two curves in Fig. 3 are obtained by using either the 1-loop running mass of Eq. (13) or the 2-loop running mass of Eq. (14) in the calculation of $\sigma_{NLO,\overline{MS}}$. This investigates the dependence of Δ_{rel} on the resummation of higher order corrections in $\overline{m_b}(\mu)$. As discussed in detail at the parton level in Sec. II B [see $\hat{\Delta}$ defined in Eq. (19)], the difference between the two schemes is scale dependent and can be very big for small and large scales. At the LHC, the relative difference can be well approximated by $\Delta_{rel}=\frac{1}{2}AB$ with $A=(\alpha_s/4\pi)g_{NLO}/g_{LO}$ and $B=[1-(\overline{m_b}/m_b)^2]$, where $g_{NLO,LO}$ correspond to the $g^{ij}_{NLO,LO}$ contributions of Eqs. (17) and (18) calculated at hadron level. This approximation can be easily verified by using these equations and neglecting the contributions of the closed fermion loops. For instance, at the LHC we find that, at $\mu=0.7\mu_0$, $A=0.28$ and $B=0.57$, while at $\mu=4\mu_0$, $A=0.92$ and $B=0.66$. The fact that A strongly depends on μ while B varies only little with μ illustrates that the difference between the $\overline{MS}$ and the *OS* schemes for the renormalization of the bottom quark is not necessarily dominated by the running of the bottom quark mass as would be the case when the majority of the NLO corrections can be absorbed in the running of m_b. This is also supported by observing that using $\overline{m_b}(\mu)_{2l}$ instead of $\overline{m_b}(\mu)_{1l}$ does not improve the μ dependence of Δ_{rel}.

In conclusion, the NLO $\overline{MS}$ cross section shows an overall better perturbative behavior, but, as the previous discussion also illustrates, the use of the $\overline{MS}$ bottom quark Yukawa coupling should not be overemphasized. It is probably a good approximation to take the difference between $\sigma_{NLO,OS}$ and $\sigma_{NLO,\overline{MS}}$ at their points of least scale sensitivity as an upper bound on the theoretical error of the NLO cross section, on top of the uncertainty due to the residual scale

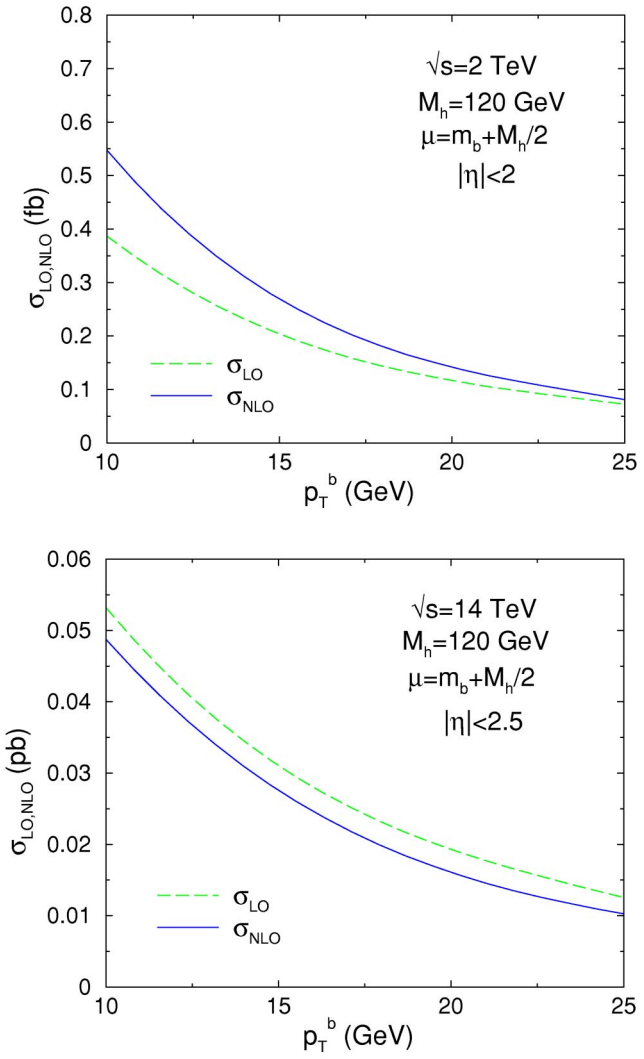

FIG. 4. $\sigma_{NLO,\overline{MS}}$ and $\sigma_{LO,\overline{MS}}$ for $p\bar{p}\to b\bar{b}h$ at $\sqrt{s}=2$ TeV (top) and for $pp\to b\bar{b}h$ at $\sqrt{s}=14$ TeV (bottom) as a function of the cut imposed on the final state bottom and antibottom transverse momentum (p_T^b), for $M_h=120$ GeV and $\mu=\mu_0=m_b+M_h/2$.

dependence. This would amount to an additional 15–20 % uncertainty arising from the dependence on the bottom quark Yukawa coupling renormalization scheme.

In Fig. 4 we illustrate the dependence of the exclusive cross section on the p_T cut imposed on the final state bottom and antibottom quarks, at both the Tevatron (top) and the LHC (bottom). We plot the LO and NLO cross sections obtained using the $\overline{MS}$ bottom quark Yukawa coupling. Reducing the p_T cut from 25 GeV to 10 GeV approximately increases the cross section by a factor of 4. However, as the p_T cut is reduced, the theoretical calculation of the cross section becomes more unstable, because the integration over the phase space of the final state bottom quarks approaches more and more a region of collinear singularities. Results without a cut on the transverse momentum of the bottom quarks will be presented in a later work [57] (see also Ref. [32]).

Finally, in Figs. 5, 6, 7, and 8 we plot the LO and NLO transverse momentum (p_T) and pseudorapidity (η) distributions of the final state particles, the bottom and antibottom quarks, and the Higgs boson, both for the Tevatron and for the LHC. Both LO and NLO differential cross sections are obtained in the SM and using the *OS* scheme for the bottom quark Yukawa coupling. For the renormalization/factorization scale we choose $\mu=2m_b+M_h$ at the Tevatron and $\mu=2(2m_b+M_h)$ at the LHC. These two scales are well within the plateau regions where the *OS* NLO cross sections vary the least with the value of μ. Similar results can be obtained using the $\overline{MS}$ bottom quark Yukawa coupling.

In Fig. 5 we show the LO and NLO p_T distributions of the bottom or antibottom quark with highest p_T, while Fig. 6 displays the p_T distributions of the SM Higgs boson. The pseudorapidity distributions of the bottom quark and the Higgs boson are shown in Fig. 7 and Fig. 8, respectively.

To illustrate the impact of the NLO corrections on the p_T and η distributions, we show in Figs. 9 and 10 the corresponding relative corrections $(d\sigma_{NLO}/dO)/(d\sigma_{LO}/dO)-1$ (in percent), for $O=p_{T,max},p_T^h,\eta_b,\eta_h$. As can be seen at least at the Tevatron, the NLO corrections considerably affect the shape of the distributions and their effect cannot be obtained from simply rescaling the LO distributions with a K-factor of $\sigma_{NLO}/\sigma_{LO}=1.38\pm0.02$ (Tevatron, $\mu=2\mu_0$) and $\sigma_{NLO}/\sigma_{LO}=1.11\pm0.03$ (LHC, $\mu=4\mu_0$).

B. MSSM results

The rate for $b\bar{b}h$ production can be significantly enhanced in a supersymmetric model with large values of $\tan\beta$. In the MSSM, the bottom and top quark couplings to the scalar Higgs bosons are given by

$$b\bar{b}h^0 \;:\; -\frac{\sin\alpha}{\cos\beta}g_{b\bar{b}h} \qquad t\bar{t}h^0 \;:\; \frac{\cos\alpha}{\sin\beta}g_{t\bar{t}h}$$

$$b\bar{b}H^0 \;:\; \frac{\cos\alpha}{\cos\beta}g_{b\bar{b}h} \qquad t\bar{t}H^0 \;:\; \frac{\sin\alpha}{\sin\beta}g_{t\bar{t}h}$$

where $g_{b\bar{b}h}$ and $g_{t\bar{t}h}$ are the SM bottom and top quark Yukawa couplings, h^0 and H^0 are the lighter and heavier neutral scalars of the MSSM, and α is the angle which diagonalizes the neutral scalar Higgs mass matrix [58]. By replacing the SM top and bottom quark Yukawa couplings with the corresponding MSSM ones, our calculation can then be straightforwardly generalized to the case of the scalar Higgs bosons of the MSSM. The bottom quark Yukawa coupling to the MSSM pseudoscalar Higgs boson, A^0, is also enhanced at large $\tan\beta$. The corresponding cross section for $b\bar{b}A^0$ production can be obtained from our calculation in the $m_b\to0$ limit, which we do not consider in this paper. We will present, however, complete results for $b\bar{b}A^0$ production, i.e. for nonzero m_b, in a future study.

The MSSM Higgs boson masses and the mixing angle α have been computed up to two-loop order using the program FEYNHIGGS [59]. In Tables I and II we provide the values of the input parameters [$(M_{h^0},\tan\beta)$ or $(M_{H^0},\tan\beta)$] and the resulting values of α used in the calculation of the top and

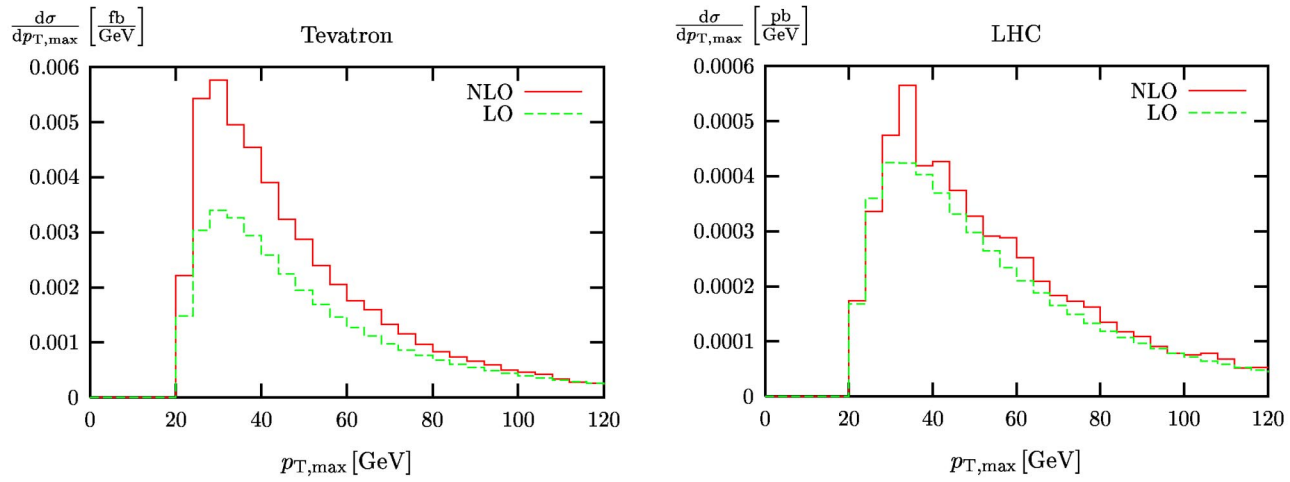

FIG. 5. Transverse momentum distributions at LO and NLO of the bottom or antibottom quark with the largest p_T. Shown are the $p_{T,max}$ distributions for $p\bar{p}\to b\bar{b}h$ production at $\sqrt{s}=2$ TeV (left) and $pp\to b\bar{b}h$ production at $\sqrt{s}=14$ TeV (right) in the SM and using the OS scheme for the bottom quark Yukawa coupling. At the Tevatron we choose $\mu=2m_b+M_h$, while at the LHC we choose $\mu=2(2m_b+M_h)$.

bottom quark Yukawa couplings to the light and heavy neutral MSSM scalar Higgs bosons. This choice of MSSM parameters takes into account present experimental limits on the MSSM parameter space, but represents otherwise just one among many possible realizations of the MSSM parameter space. The results obtained with this choice of MSSM input parameters illustrate the typical enhancements over the SM results one can expect when considering the production of neutral scalar Higgs bosons in association with bottom quarks.

The top part of Fig. 11 compares the NLO $p\bar{p}\to b\bar{b}h$ SM cross section at the Tevatron with the corresponding cross section for production of the lightest neutral scalar Higgs boson in the MSSM for $\tan\beta=10$, 20, and 40. A large enhancement of up to three orders of magnitude is observed. As the light neutral Higgs boson mass approaches its maximum value, the mixing angle α becomes very small, as can be clearly seen in Table I. This has the effect of suppressing the $b\bar{b}h^0$ rates at this point. A similar effect can be observed in the production of a heavy neutral Higgs boson when M_{H^0} is approaching its minimum value (see Table II), as shown in the bottom part of Fig. 11. Again, we compare the production of the SM Higgs boson with that of the heavier neutral scalar Higgs boson of the MSSM and observe a significant enhancement of the rate in the MSSM for large $\tan\beta$.

IV. CONCLUSIONS

We presented results for the next-to-leading order QCD cross section for exclusive $b\bar{b}h$ production at both the Tevatron and the LHC. Our NLO results show an improved sta-

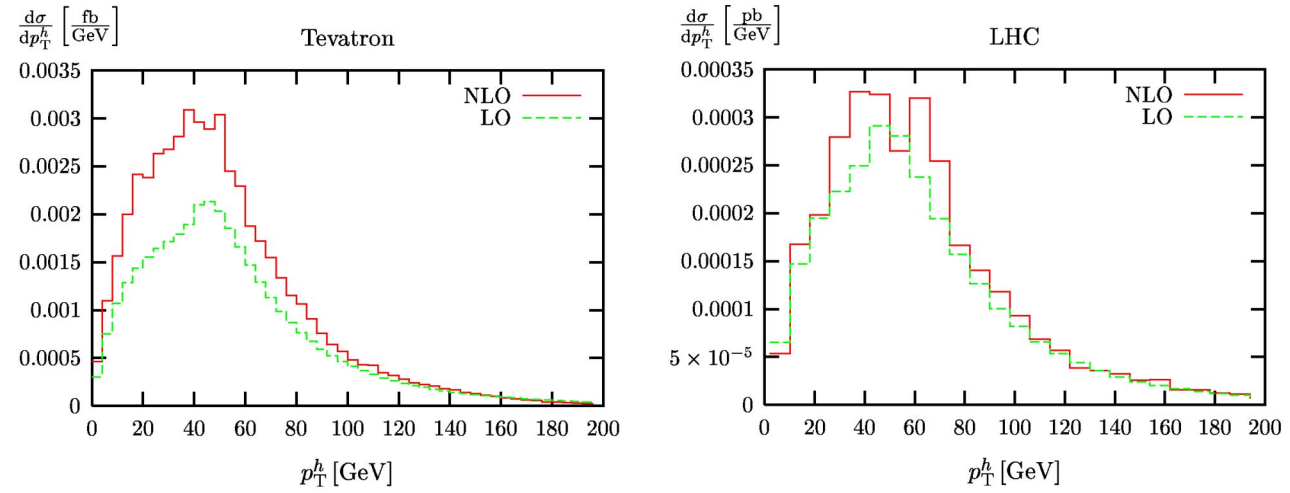

FIG. 6. Transverse momentum distributions at LO and NLO of the SM Higgs boson. Shown are the p_T^h distributions for $p\bar{p}\to b\bar{b}h$ production at $\sqrt{s}=2$ TeV (left) and $pp\to b\bar{b}h$ production at $\sqrt{s}=14$ TeV (right) in the SM and using the OS scheme for the bottom quark Yukawa coupling. At the Tevatron we choose $\mu=2m_b+M_h$, while at the LHC we choose $\mu=2(2m_b+M_h)$.

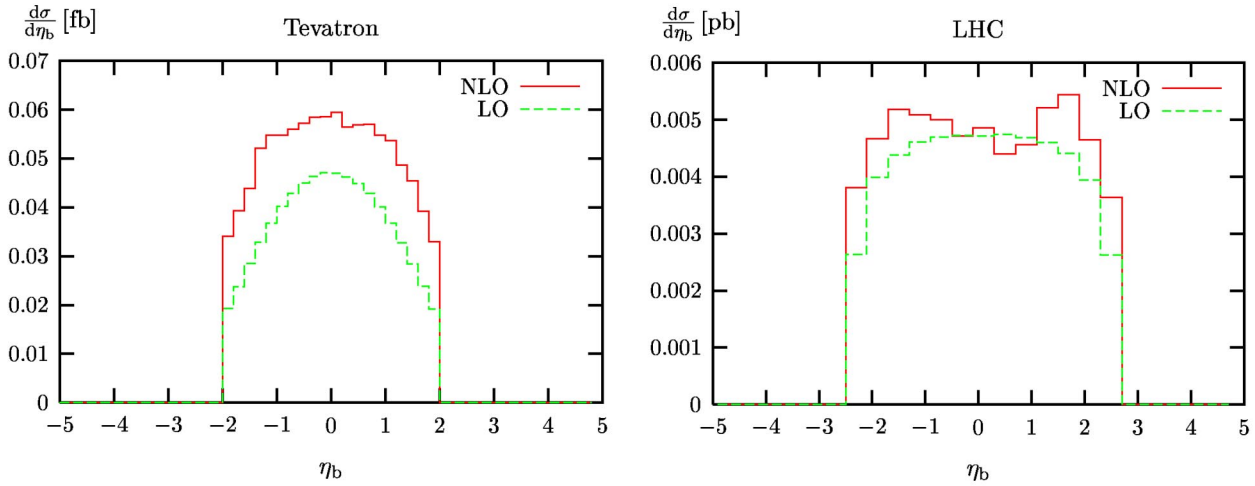

FIG. 7. Pseudorapidity distributions at LO and NLO of the bottom quark. Shown are the η_b distributions for $p\bar{p}\to b\bar{b}h$ production at $\sqrt{s}=2$ TeV (left) and $pp\to b\bar{b}h$ production at $\sqrt{s}=14$ TeV (right) in the SM and using the OS scheme for the bottom quark Yukawa coupling. At the Tevatron we choose $\mu=2m_b+M_h$, while at the LHC we choose $\mu=2(2m_b+M_h)$.

bility with respect to the unphysical factorization and renormalization scales as compared to the leading order results and increase the reliability of the theoretical prediction. The uncertainty in the resummation of large logarithms from higher order corrections, however, is also visible in the dependence of the NLO cross section on the renormalization scheme of the bottom quark Yukawa coupling. The residual renormalization/factorization scale dependence is of the order of 15–20 % when the bottom quark Yukawa coupling is renormalized in the *OS* or $\overline{MS}$ schemes respectively. We conservatively estimate the additional uncertainty due to the renormalization scheme dependence of the bottom quark Yukawa coupling to be at most of order 15–20 %.

Our calculation is important for Higgs boson searches at hadron colliders where two high p_T bottom quarks are tagged in the final state. In supersymmetric models with large $\tan\beta$, $b\bar{b}h$ production can be an important discovery channel, at both the Tevatron and the LHC.

ACKNOWLEDGMENTS

We thank R. Harlander, M. Krämer, J. Kühn, F. Maltoni, and S. Willenbrock for valuable discussions. S.D. and L.R. would like to thank the organizers of the Les Houches Workshop on *Physics at TeV Colliders* for providing such a pleasant and stimulating environment where many of the issues presented in this paper were extensively discussed. L.R. acknowledges the kind hospitality of the Theory Division at CERN and of the Particle Physics group of the IST in Lisbon while part of this work was being completed. The work of S.D. (C.B.J. and L.R.) is supported in part by the U.S. De-

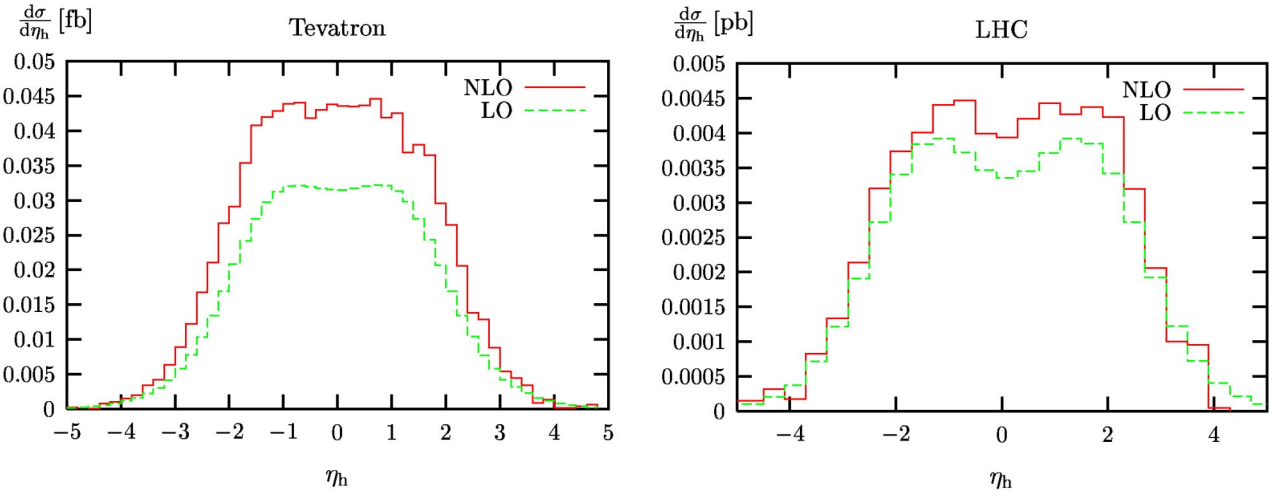

FIG. 8. Pseudorapidity distributions at LO and NLO of the SM Higgs boson. Shown are the η_h distributions for $p\bar{p}\to b\bar{b}h$ production at $\sqrt{s}=2$ TeV (left) and $pp\to b\bar{b}h$ production at $\sqrt{s}=14$ TeV (right) in the SM and using the OS scheme for the bottom quark Yukawa coupling. At the Tevatron we choose $\mu=2m_b+M_h$, while at the LHC we choose $\mu=2(2m_b+M_h)$.

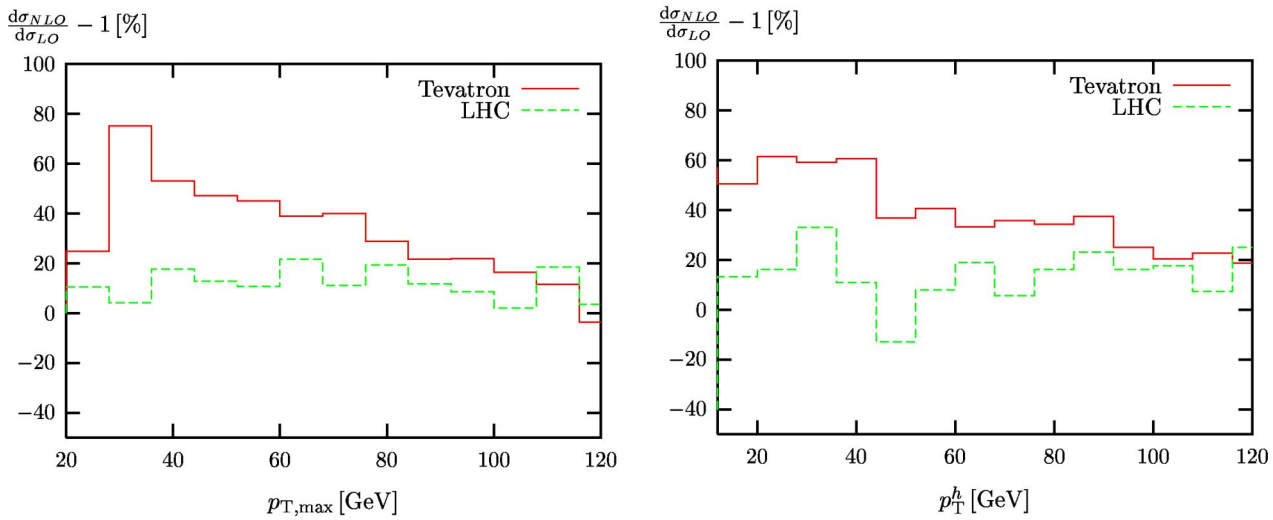

FIG. 9. The relative corrections $d\sigma_{NLO}/d\sigma_{LO}-1$ for the $p_{T,max}$ (left) and p_T^h (right) distributions to $b\bar{b}h$ production at the Tevatron and the LHC as shown in Fig. 5 and Fig. 6, respectively.

partment of Energy under grant DE-AC02-98CH10886 (DE-FG02-97ER41022). The work of D.W. is supported in part by the National Science Foundation under grant No. PHY-0244875.

APPENDIX A: RENORMALIZATION COUNTERTERMS

In this appendix, we summarize the explicit form of the renormalization counterterms used in this calculation. The conventions are identical to those adopted in our previous calculations of the NLO cross section for hadronic $t\bar{t}h$ production [13,15]. This appendix is meant to complement Sec. II B and is presented here only for the reader's convenience.

As already explained in Sec. II B, we fix the renormalization scheme of $\delta Z_2^{(q)}$, δZ_3, and δZ_{α_s}, while we consider two different renormalization schemes (*OS* and $\overline{MS}$) for $\delta Z_2^{(b)}$ and δm_b.

When using the *OS* schemes, the bottom wave function and mass counterterms are given by

$$(\delta Z_2^{(b)})_{OS} = -\frac{\alpha_s}{4\pi} C_F \left(\frac{4\pi\mu^2}{m_b^2}\right)^{\epsilon} \Gamma(1+\epsilon)\left(\frac{1}{\epsilon_{UV}} + 4 + \frac{2}{\epsilon_{IR}}\right), \tag{A1}$$

$$\left(\frac{\delta m_b}{m_b}\right)_{OS} = -\frac{\alpha_s}{4\pi} C_F \left(\frac{4\pi\mu^2}{m_b^2}\right)^{\epsilon} \Gamma(1+\epsilon)\left(\frac{3}{\epsilon_{UV}} + 4\right), \tag{A2}$$

while in the $\overline{MS}$ scheme we have that

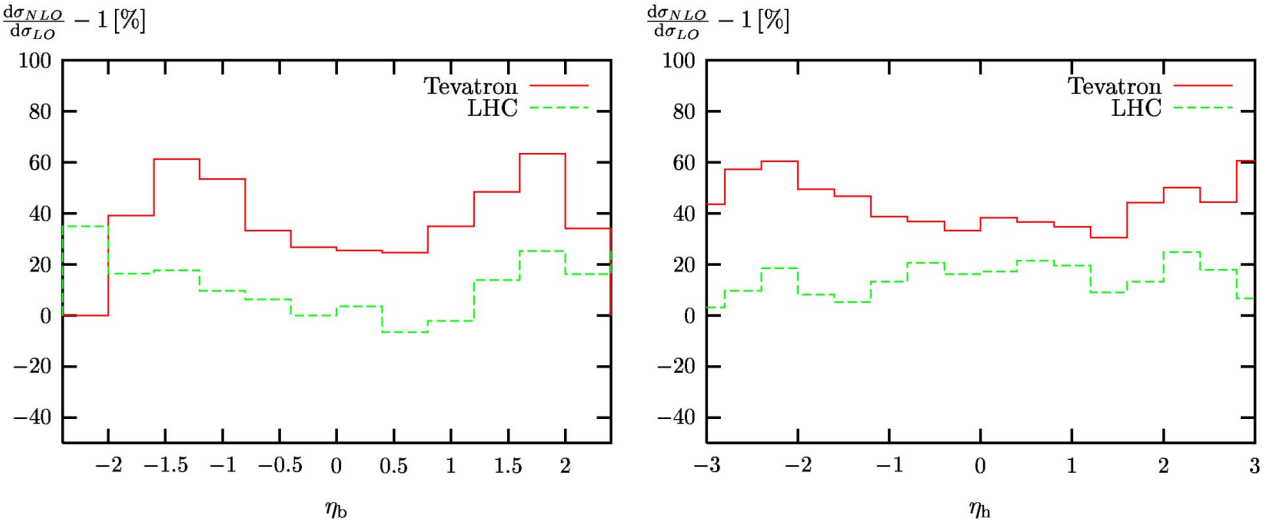

FIG. 10. The relative corrections $d\sigma_{NLO}/d\sigma_{LO}-1$ for the η_b (left) and η_h (right) distributions to $b\bar{b}h$ production at the Tevatron and the LHC as shown in Fig. 7 and Fig. 8, respectively.

TABLE I. Values of α and M_A, computed up to two-loop order by using the program FEYNHIGGS [59], corresponding to different choices of $\tan\beta$ and M_{h^0}. In the calculation of α and M_A we choose the genuine SUSY input parameters as follows: $M_{\tilde{g}}=M_{\tilde{t}_L}=M_{\tilde{t}_R}=M_{\tilde{b}_L}=M_{\tilde{b}_R}=1$ TeV, $M_t^{LR}=2$ TeV, $A_b=A_t=M_t^{LR}+\mu\cot\beta$, and $\mu=M_2=200$ GeV.

		$\tan\beta=10$		
M_{h^0} [GeV]	100	110	120	130
M_A [GeV]	102.42	113.86	127.95	264.72
α [rad]	−1.3249	−1.1963	−0.9054	−0.1463
		$\tan\beta=20$		
M_{h^0} [GeV]	100	110	120	130
M_A [GeV]	100.61	110.95	121.89	146.72
α [rad]	−1.4420	−1.3707	−1.1856	−0.3108
		$\tan\beta=40$		
M_{h^0} [GeV]	100	110	120	130
M_A [GeV]	100.15	110.23	120.46	133.71
α [rad]	−1.5007	−1.4601	−1.3444	−0.4999

$$(\delta Z_2^{(b)})_{\overline{MS}}=-\frac{\alpha_s}{4\pi}C_F(4\pi)^{\epsilon}\Gamma(1+\epsilon)\frac{1}{\epsilon_{UV}}, \tag{A3}$$

$$\left(\frac{\delta m_b}{m_b}\right)_{\overline{MS}}=-\frac{\alpha_s}{4\pi}C_F(4\pi)^{\epsilon}\Gamma(1+\epsilon)\frac{3}{\epsilon_{UV}}, \tag{A4}$$

TABLE II. Values of α and M_A, computed up to two-loop order by using the program FEYNHIGGS [59], corresponding to different choices of $\tan\beta$ and M_{H^0}. In the calculation of α and M_A we choose the genuine SUSY input parameters as follows: $M_{\tilde{g}}=M_{\tilde{t}_L}=M_{\tilde{t}_R}=M_{\tilde{b}_L}=M_{\tilde{b}_R}=1$ TeV, $M_t^{LR}=0$, $A_b=A_t=M_t^{LR}+\mu\cot\beta$, and $\mu=M_2=1$ TeV.

			$\tan\beta=10$		
M_{H^0} [GeV]	120	200	400	600	800
M_A [GeV]	108.05	198.55	399.41	599.64	799.74
α [rad]	−0.9018	−0.1762	−0.1140	−0.1057	−0.1030
			$\tan\beta=20$		
M_{H^0} [GeV]	120	200	400	600	800
M_A [GeV]	116.45	199.56	399.81	599.89	799.91
α [rad]	−0.5785	−0.0901	−0.0574	−0.0531	−0.0517
			$\tan\beta=40$		
M_{H^0} [GeV]	120	200	400	600	800
M_A [GeV]	118.92	199.82	399.92	599.95	799.96
α [rad]	−0.3116	−0.0460	−0.0289	−0.0267	−0.0259

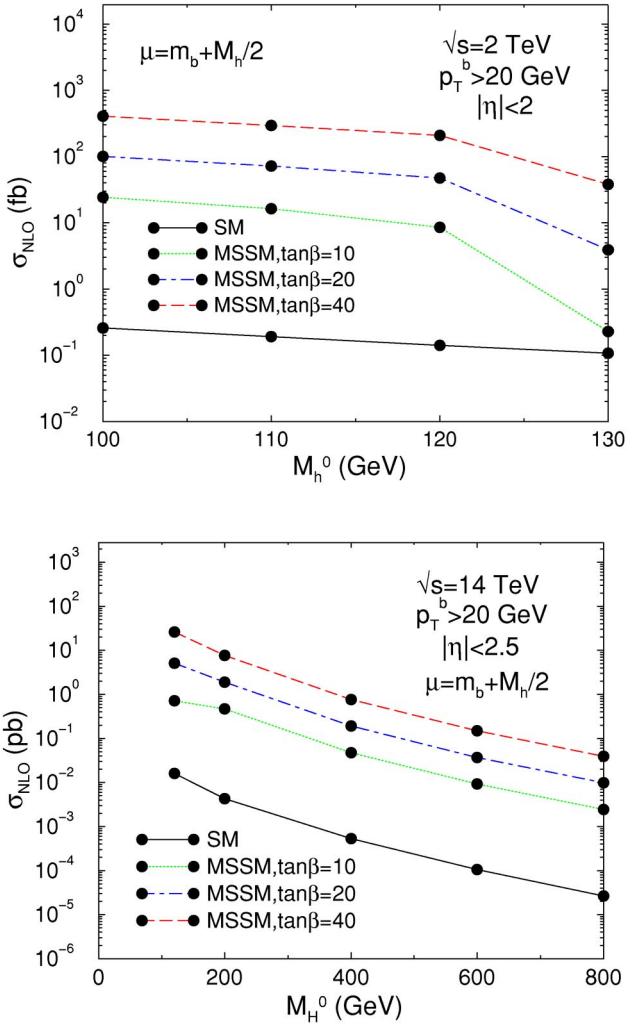

FIG. 11. $\sigma_{NLO,\overline{MS}}$ for $p\bar{p}\to b\bar{b}h$ production at $\sqrt{s}=2$ TeV (top) and $pp\to b\bar{b}h$ production at $\sqrt{s}=14$ TeV (bottom) in the SM and in the MSSM with $\tan\beta=10$, 20, and 40. For the Tevatron we considered $p\bar{p}\to b\bar{b}h^0$ with $M_{h^0}=100,110,120$, and 130 GeV, while for the LHC we considered $pp\to b\bar{b}H^0$ with $M_{H^0}=120,200,400,600$, and 800 GeV. For each $(M_{h^0},\tan\beta)$ and $(M_{H^0},\tan\beta)$ point, the corresponding values of α and M_A are listed in Tables I and II.

where $C_F=(N^2-1)/2/N$ and $N=3$ is the number of colors. We have explicitly distinguished between ultraviolet and infrared divergences. The infrared divergences are cancelled between virtual and real soft and collinear contributions according to the pattern outlined in Refs. [13,15], to which we refer for more details.

For the case of massless external quarks, we always use the wave function renormalized in the on-shell scheme as given by

$$\delta Z_2^{(q)}=-\left(\frac{\alpha_s}{4\pi}\right)\left(\frac{4\pi\mu^2}{s}\right)^{\epsilon}\Gamma(1+\epsilon)C_F\left(\frac{1}{\epsilon_{UV}}-\frac{1}{\epsilon_{IR}}\right). \tag{A5}$$

The wave-function of external gluons is renormalized in the $\overline{MS}$ subtraction scheme for $n_{lf}=5$ light flavors,

$$\delta Z_3 = \frac{\alpha_s}{4\pi}(4\pi)^{\epsilon}\Gamma(1+\epsilon)\left\{\left(\frac{5}{3}N - \frac{2}{3}n_{lf}\right)\frac{1}{\epsilon_{UV}} - \frac{2}{3}\left[\frac{1}{\epsilon_{UV}} + \ln\left(\frac{\mu^2}{m_t^2}\right)\right]\right\}, \tag{A6}$$

according to which we also need to consider the insertion of a finite self-energy correction on the external gluon legs as discussed in detail in Ref. [15]. For the renormalization of α_s we use the $\overline{MS}$ scheme, modified to decouple the top quark [52,53]. The first n_{lf} light flavors are subtracted using the $\overline{MS}$ scheme, while the divergences associated with the top-quark loop are subtracted at zero momentum,

$$\delta Z_{\alpha_s} = \frac{\alpha_s}{4\pi}(4\pi)^{\epsilon}\Gamma(1+\epsilon)\left\{\left(\frac{2}{3}n_{lf} - \frac{11}{3}N\right)\frac{1}{\epsilon_{UV}} + \frac{2}{3}\left[\frac{1}{\epsilon_{UV}} + \ln\left(\frac{\mu^2}{m_t^2}\right)\right]\right\}, \tag{A7}$$

such that, in this scheme, the renormalized strong coupling constant $\alpha_s(\mu)$ evolves with $n_{lf}=5$ light flavors.

The counterterms contribute to the NLO parton-level total cross section of Eq. (2) as follows:

$$\delta\hat{\sigma}^{q\bar{q}}_{NLO,CT} = 2\hat{\sigma}^{q\bar{q}}_{LO}\left[\delta Z_2^{(q)} + \delta Z_2^{(b)} + \frac{\delta m_b}{m_b} + \delta Z_{\alpha_s}\right], \tag{A8}$$

$$\delta\hat{\sigma}^{gg}_{NLO,CT} = 2\hat{\sigma}^{gg}_{LO}\left[\delta Z_2^{(b)} + \frac{\delta m_b}{m_b} + \delta Z_{\alpha_s} + \delta Z_3\right], \tag{A9}$$

and the ultraviolet divergences are cancelled when these contributions are combined with the rest of the $O(\alpha_s^3)$ virtual cross section.

[1] LEP Higgs Working Group, R. Barater *et al.*, Phys. Lett. B **565**, 61 (2003).
[2] LEP Electroweak Working Group, talk presented by P. Wells, EPS-HEP Conference, Aachen, Germany, 2003. See also LEP EWWG web site at http://lepewwg.web.cern.ch/LEPEWWG/.
[3] LEP Higgs Working Group, Note/2001-04, hep-ex/0107030.
[4] T. Han and S. Willenbrock, Phys. Lett. B **273**, 167 (1991).
[5] T. Han, G. Valencia, and S. Willenbrock, Phys. Rev. Lett. **69**, 3274 (1992).
[6] S. Dawson, Nucl. Phys. **B359**, 283 (1991).
[7] A. Djouadi, M. Spira, and P.M. Zerwas, Phys. Lett. B **264**, 440 (1991).
[8] D. Graudenz, M. Spira, and P.M. Zerwas, Phys. Rev. Lett. **70**, 1372 (1993).
[9] M. Spira, A. Djouadi, D. Graudenz, and P.M. Zerwas, Nucl. Phys. **B453**, 17 (1995).
[10] W. Beenakker, S. Dittmaier, M. Krämer, B. Plümper, M. Spira, and P. Zerwas, Phys. Rev. Lett. **87**, 201805 (2001).
[11] L. Reina and S. Dawson, Phys. Rev. Lett. **87**, 201804 (2001).
[12] W. Beenakker, S. Dittmaier, M. Krämer, B. Plümper, M. Spira, and P. Zerwas, Nucl. Phys. **B653**, 151 (2003).
[13] L. Reina, S. Dawson, and D. Wackeroth, Phys. Rev. D **65**, 053017 (2002).
[14] S. Dawson, L.H. Orr, L. Reina, and D. Wackeroth, Phys. Rev. D **67**, 071503(R) (2003).
[15] S. Dawson, C. Jackson, L.H. Orr, L. Reina, and D. Wackeroth, Phys. Rev. D **68**, 034022 (2003).
[16] R.V. Harlander and W.B. Kilgore, Phys. Rev. Lett. **88**, 201801 (2002).
[17] C. Anastasiou and K. Melnikov, Nucl. Phys. **B646**, 220 (2002).
[18] R.V. Harlander and W.B. Kilgore, Phys. Rev. D **64**, 013015 (2001).
[19] S. Catani, D. de Florian, and M. Grazzini, J. High Energy Phys. **05**, 025 (2001).
[20] V. Ravindran, J. Smith, and W.L. Van Neerven, Nucl. Phys. **B665**, 325 (2003).
[21] O. Brein, A. Djouadi, and R. Harlander, Phys. Lett. B **579**, 149 (2004).
[22] D.A. Dicus and S. Willenbrock, Phys. Rev. D **39**, 751 (1989).
[23] R.V. Harlander and W.B. Kilgore, Phys. Rev. D **68**, 013001 (2003).
[24] D. Dicus, T. Stelzer, Z. Sullivan, and S. Willenbrock, Phys. Rev. D **59**, 094016 (1999).
[25] C. Balazs, H.-J. He, and C.P. Yuan, Phys. Rev. D **60**, 114001 (1999).
[26] D. Rainwater, M. Spira, and D. Zeppenfeld, hep-ph/0203187.
[27] T. Plehn, Phys. Rev. D **67**, 014018 (2003).
[28] F. Maltoni, Z. Sullivan, and S. Willenbrock, Phys. Rev. D **67**, 093005 (2003).
[29] E. Boos and T. Plehn, Phys. Rev. D (to be published), hep-ph/0304034.
[30] Talk presented by M. Krämer, in *Workshop on the Physics of TeV Colliders*, Les Houches, France, 2003.
[31] Talk presented by M. Spira, in *CERN Workshop on Monte Carlo Tools for the LHC*, CERN, Geneva, Switzerland, 2003.
[32] S. Dittmaier, M. Krämer, and M. Spira, hep-ph/0309204.
[33] CMS Collaboration, Technical Proposal, CERN/LHCC/94-38, 1994.
[34] V.D. Barger and C. Kao, Phys. Lett. B **424**, 69 (1998).
[35] E. Richter-Was *et al.*, Int. J. Mod. Phys. A **13**, 1371 (1998).
[36] ATLAS Collaboration, Technical Design Report, Vol. II, CERN/LHCC/99-15, 1999.
[37] M. Carena, S. Mrenna, and C.E.M. Wagner, Phys. Rev. D **60**, 075010 (1999).

[38] J. Campbell, R.K. Ellis, F. Maltoni, and S. Willenbrock, Phys. Rev. D **67**, 095002 (2003).
[39] J. Dai, J.F. Gunion, and R. Vega, Phys. Lett. B **345**, 29 (1995).
[40] J. Dai, J.F. Gunion, and R. Vega, Phys. Lett. B **387**, 801 (1996).
[41] CDF Collaboration, T. Affolder *et al.*, Phys. Rev. Lett. **86**, 4472 (2001).
[42] Report of the Tevatron Higgs Working Group, M. Carena *et al.*, hep-ph/0010338.
[43] C. Balazs, J.L. Diaz-Cruz, H.J. He, T. Tait, and C.P. Yuan, Phys. Rev. D **59**, 055016 (1999).
[44] E. Richter-Was and D. Froidevaux, Z. Phys. C **76**, 665 (1997).
[45] S. Dawson, D. Dicus, and C. Kao, Phys. Lett. B **545**, 132 (2002).
[46] E. Boos, A. Djouadi, and A. Nikitenko, Phys. Lett. B **578**, 384 (2004).
[47] E. Braaten and J.P. Leveille, Phys. Rev. D **22**, 715 (1980).
[48] M. Drees and K.-i. Hikasa, Phys. Lett. B **240**, 455 (1990).
[49] S.G. Gorishnii, A.L. Kataev, and S.A. Larin, Sov. J. Nucl. Phys. **40**, 329 (1984).
[50] A.L. Kataev and V.T. Kim, Mod. Phys. Lett. A **9**, 1309 (1994).
[51] Talks presented by L. Reina, in *Workshop on the Physics of TeV Colliders*, Les Houches, France, 2003; *QCD 2003*, Montpellier, France, 2003; *EPS 2003*, Aachen, Germany, 2003.
[52] J.C. Collins, F. Wilczek, and A. Zee, Phys. Rev. D **18**, 242 (1978).
[53] P. Nason, S. Dawson, and R.K. Ellis, Nucl. Phys. **B327**, 49 (1989).
[54] H. Lehmann, K. Symanzik, and W. Zimmermann, Nuovo Cimento **1**, 205 (1955).
[55] G. Altarelli and G. Parisi, Nucl. Phys. **B126**, 298 (1977).
[56] CTEQ Collaboration, H.L. Lai *et al.*, Eur. Phys. J. C **12**, 375 (2000).
[57] S. Dawson, C. Jackson, L. Reina, and D. Wackeroth, in preparation.
[58] J. F. Gunion, H. E. Haber, G. L. Kane, and S. Dawson, *The Higgs Hunter's Guide* (Addison-Wesley, Menlo Park, NJ, 1990), SCIPP-89/13.
[59] S. Heinemeyer, W. Hollik, and G. Weiglein, Comput. Phys. Commun. **124**, 76 (2000); we used version 1.3.1 (December 2002). For details see FEYNHIGGS web site at http://www.feynhiggs.de/FeynHiggs.html, hep-ph/9812320.